RSC Advances

PAPER

View Article Online
View Journal | View Issue

Cite this: *RSC Adv.*, 2014, **4**, 57823

Charge density distribution and electrostatic interactions of ethionamide: an inhibitor of the enoyl acyl carrier protein reductase (inhA) enzyme of *Mycobacterium tuberculosis*†

G. Rajalakshmi,[a] Mysore S. Pavan[b] and P. Kumaradhas*[a]

Received 1st August 2014
Accepted 16th September 2014

DOI: 10.1039/c4ra07953a

www.rsc.org/advances

An experimental charge density analysis of an anti-TB drug ethionamide was carried out from high resolution X-ray diffraction at 100 K to understand its charge density distribution and electrostatic properties. The experimental results were validated from periodic theoretical charge density calculations performed using CRYSTAL09 at the B3LYP/6-31G** level of theory. The electron density $\rho_{bcp}(r)$ and the Laplacian of electron density $\nabla^2\rho_{bcp}(r)$ of the molecule calculated from both the methods display the charge density distribution of the ethionamide molecule in the crystal field. The electrostatic potential map shows a large electropositive region around the pyridine ring and a large electronegative region at the vicinity of the thiol atom. The calculated experimental dipole moment is 10.6*D*, which is higher than the value calculated from theory (8.2*D*). The topological properties of C–H···S, N–H···N and N–H···S hydrogen bonds were calculated, revealing their strength. The charge density analysis of the ethionamide molecule determined from both the experiment and theory gives the topological and electrostatic properties of the molecule, which allows to precisely understand the nature of intra and intermolecular interactions.

Introduction

Tuberculosis remains the second leading infectious disease[1] causing high mortality worldwide. Isoniazid, ethambutol, rifampicin and pyrazinamide are the first line drugs being used for the treatment at the initial stage of *Mycobacterium tuberculosis* disease.[2] These first line drugs are less effective for the treatment of multidrug resistance tuberculosis (MDR-TB).[3] Drugs such as thioamides, ethionamide (ETH), and prothionamide are more effective against the MDR-TB; of these, ETH is the more efficacious, cheap and easily available drug, and is one of the second line drugs and the structural analogue of isoniazid (INH).[4,5] ETH is also a prodrug (Fig. 1), it should be activated by the enzyme to exert its antimicrobial activity.[6] The enzyme flavinmonooxygenase (FMO) ethA[7] activates the ETH. EthA oxidizes the ETH moiety to form the ETH–SO metabolite and 2-ethyl-4-amidopyridine, exhibiting biological activity similar to the parent drug.[8] *In vitro* studies have identified other metabolites such as ETH–nitrite, ETH–aldehyde and ETH–OH.[9–11] The proposed active form of ETH is shown in Fig. 1.

Similar to INH, ETH also targets the enoyl acyl carrier protein reductase (inhA) enzyme and inhibits the synthesis of mycolic acid.[12,13] The mutations in the ethA gene show resistance to ETH; hence, it is essential to discover a new drug to target the inhA without activation by ethA enzyme.[14] Fig. 1 shows the molecular structure of ETH and its reactive species (ethionamide S-oxide and 2-ethyl-4-amidopyridine). In recent years, some derivatives of ETH drug molecules were synthesized and characterised in the quest to design anti-TB drugs with enhanced pharmacological activity. However, to the best of our knowledge, there is no quantitative structural analysis of such drugs that has been reported yet, so it is of the utmost importance to understand the structure-activity relationship. The rational drug design requires precise knowledge about the drug–receptor interaction.

The structure, conformation and charge density distribution of drug molecules play a very important role on the binding of the same in the active site of the receptor. Further, the biological recognition between drug and the receptor is achieved by intermolecular interactions, and it mainly relies on the steric and complementary electronic properties.[15] Predicting such information from X-ray diffraction is immensely useful to derive potential lead compounds from the existing drug molecules. In this context, the conventional X-ray structure analysis provides

[a]*Laboratory of Biocrystallography and Computational Molecular Biology, Department of Physics, Periyar University, Salem 636 011, India. E-mail: kumaradhas@yahoo.com; Fax: +91-427-2345565; Tel: +91-427-2345520*

[b]*Solid State and Structural Chemistry Unit, Indian Institute of Science, Bangalore 560 012, India*

† Electronic supplementary information (ESI) available. CCDC 1000256. For ESI and crystallographic data in CIF or other electronic format see DOI: 10.1039/c4ra07953a

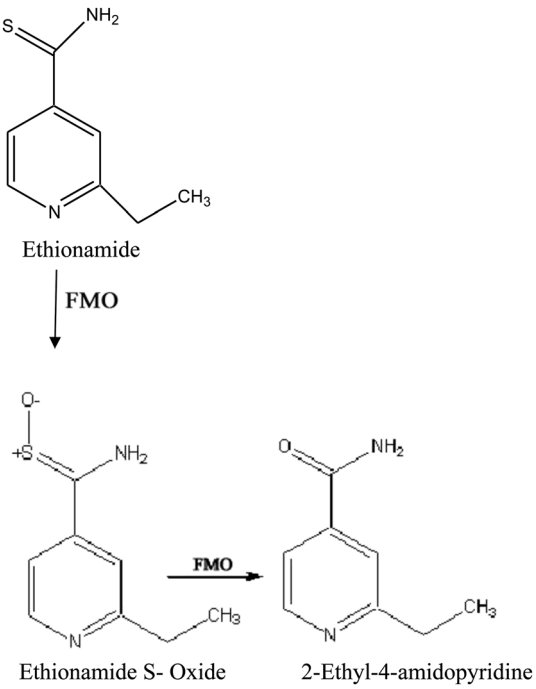

Fig. 1 Ethionamide and its reactive components: ethionamide S-oxide and 2-ethyl-4-amidopyridine.[11]

the accurate molecular geometry and the geometry of hydrogen bonding interactions, π-stacking interactions and van der Waals interactions, *etc.* However, to obtain accurate electronic structure, one has to rely on the technique of experimental charge density analysis, which unravels the structure of molecules at the electronic level allowing one to understand the charge density distribution and electrostatic properties of molecules in the crystalline environment. The electrostatic properties (atomic charge, electrostatic potential and dipole moment) can be obtained from the experimental charge density analysis, which is an important property to predict the molecular recognition and reactivity; because, it depends on the electrostatic complementarity principle.[16] It is also widely used in biological sciences to understand the structural features.[17] In the present study, we have carried out the charge density analysis of ETH by high resolution X-ray diffraction measured at 100 K. The topological properties of electron density at the bond critical points (bcp) were determined; the electron density and the corresponding Laplacian of electron density at the bcp gives the charge density distribution of the molecules. The charge density distribution of the molecule is very sensitive to intermolecular interactions. The strength of each intermolecular interaction of ETH has been characterized using the topological analysis of electron density. The electrostatic properties of the molecule have been determined. Importantly, they display the electrostatic surface of the molecule, which allows the identification of the possible reactive locations of the ETH molecule; such locations of the molecule may interact with the complementary groups of the amino acids present in the active site of receptor to inhibit/kill the *Mycobacteria*. Experimental results have been compared with the periodic theoretical calculations of ETH molecule.

Experimental

The powder form of ETH compound was obtained from Sigma-Aldrich. It was crystallized from a saturated solution of ethanol solvent at room temperature using the slow evaporation technique. Thus, grown ETH crystals are found to be yellow in colour and exhibit good morphology with high transparency. From that, a high quality single crystal was chosen and mounted in a Hampton Research Cryo-loop using paratone-N oil for high resolution X-ray diffraction intensity measurements. The crystal was cooled by cold nitrogen gas stream to 100 K by using an Oxford Cryostream N_2 open-flow crysostat. The X-ray diffraction data was collected by using CrysAlisPro diffractometer[18] using MoKα radiation and the data was reduced by using the CrysAlisPro software.[18] The high resolution data was collected up to the maximum resolution $(\sin\theta/\lambda)_{max} = 1.1$ Å^{-1}. The total number of reflections measured was 54 090; further, the reflections were sorted, merged and scaled by using SORTAV.[19] After merging, 8769 unique reflections ($I \geq 2\sigma$) were recovered to a resolution of $(\sin\theta/\lambda)_{max} = 1.1$ Å^{-1}. The internal agreement factor for the final data set is $R_{int} = 0.0406$ and $R_{sigma} = 0.024$. The crystal structure was solved and refined by using spherical atom approximation F^2 method using SHELXS-97[20] and SHELXL-97[20] software, respectively. Absorption correction was carried out by the numerical absorption correction based on Gaussian integration over a multifaceted crystal model as $\mu = 0.336$ mm^{-1}. The hydrogen bonding interactions were plotted using the PLATON[21] software.†

Multipole refinement

The electron density of ETH was modelled using the Hansen–Coppens multipole formalism implemented in XD2006.[22] In the Hansen–Coppens model,[23] electron density of each atom is represented as a sum of core electron density (ρ_{core}), a spherical valence electron density (ρ_{val}), and an aspherical part of the atomic electron density. R_l are appropriate radial functions and Y_{lm} represents the spherical harmonics. κ is the contraction–expansion parameter that modifies the radial distribution of valence electron density and κ' are the expansion and contraction parameters of the radial part of aspherical valence shell. P_{lm} is the multipole population parameters.

$$\rho_{atom}(r) = P_c\rho_c(r) + P_v\kappa^3\rho_v(\kappa r) + \sum_{l=0}^{l_{max}} \kappa'^3 R_l(\kappa' r) \sum_{m=0}^{l} P_{lm\pm} Y_{lm\pm}(\theta,\phi)$$

Because the space group of ETH crystal is *Ia*, it is non-centrosymmetric in nature; hence the origin was fixed[24] with reference to the co-ordinates of the sulphur atom S(1). During the refinements, a single scale factor was refined for the entire resolution range of data. Subsequently, a high order refinement ($\sin\theta/\lambda > 0.8$ Å^{-1}) was performed to obtain the accurate

positional and thermal parameters. During the high order refinement, the X–H bond lengths were constrained to the neutron diffraction values.[25]

During the multipole refinements, the sulphur atom was truncated at the hexadecapole level while for C and O atoms the refinement was performed upto the octupole level. κ and κ' for atoms with different chemical environments were assigned. For hydrogen atoms, the valence population and the bond directed dipole d_z were refined initially. Subsequently, the geometry obtained from high order refinement was used to obtain the anisotropic thermal displacement parameters of hydrogen atom by using the SHADE2 (ref. 26) approach. Thus, the obtained ADP's of hydrogen atoms were fixed and the bond directed quadrupoles ($q_{3z}^2 - 1$) of all hydrogen atoms were refined in the multipole modelling. For H atoms, the κ and κ' were fixed as 1.2. Geometrical parameters such as bond lengths, bond angles and torsion angles were calculated from the XDGEOM routine of XD2006.[22] The topological properties of the electron density of ETH molecule were derived from the XDPROP routine of XD2006.[22] The Hirshfeld rigid bond test[27] was performed for all the covalent bonds, and it shows that the largest difference of mean-square displacement amplitude (DMSDA) is less than 5×10^{-4} Å^2, which is an indicator of the quality of data; further, from the value of DMSDA, it can be concluded that the atomic thermal motion of ETH has been well deconvoluted. The electrostatic potential (ESP) map has been plotted using the XDGRAPH routine of XD2006.[22] The shown amino acids are the pictorial representation which are interacting with ETH in the active site.

Theoretical calculations

A periodic theoretical calculation was performed for the ETH molecule using CRYSTAL09,[28,29] in which the molecular geometry obtained from the experimental multipole refinement was used as an initial geometry. The quantum chemical calculation was carried out using the (DFT) B3LYP method[30] with the basis set 6-31G**.[31] The shrinking factors (IS1–IS3) along the reciprocal lattice vectors were set at 4 (30 *K* points in the irreducible Brillouin zone). The truncation parameters were set as ITOL1 = ITOL2 = ITOL3 = ITOL4 = 6 and ITOL5 = 14. For better convergence, the level shifter value was set to 0.6 Hartrees per cycle. The atomic position was fixed to the values obtained from the experiment. Multipole refinement for the theoretical structure factors was also carried out as the multipoles used in the experiment. Further, the topological and electrostatic properties were calculated and compared with the experimental results.

Results and discussion

Molecular structure and intermolecular interactions

Fig. 2 displays the ORTEP[32] view of ETH molecule. The C–C bond lengths of ETH molecule containing pyridine ring ranges from 1.3939(4) to 1.4029(3) Å, and the average value is 1.3993 Å. The bond length of the C(1)–C(8) and C(4)–C(6) bonds are 1.4984(3), 1.5145(4) Å respectively; the C_{sp^3}–C_{sp^3} bond length of the C(6)–C(7) bond is 1.5281(5) Å. The S(1)–C(8) bond length is 1.6849(3) Å, which almost agrees with the reported bond length of room temperature structure.[33] The bond angle of the amide group H(2A)–N(2)–H(2B) is 118.4(3)°, which is larger than the usual NH_2 bond angle. This difference is attributed to the involvement of hydrogen atoms H(2A) and H(2B) in hydrogen bonding interactions. The torsion angle of C(5)–C(1)–C(8)–S(1) is −150.5(1)°; this wide angle bond twist indicates that this bond exhibit a *trans* conformation.

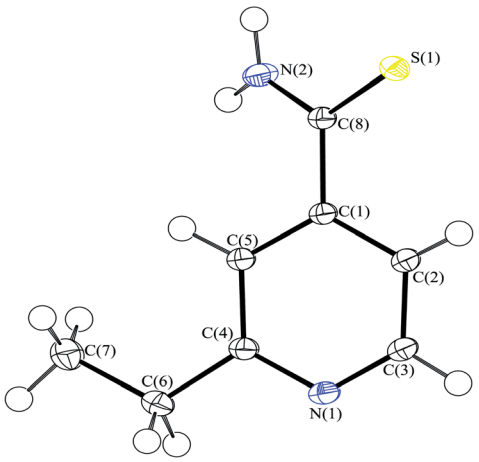

Fig. 2 ORTEP view of the ethionamide molecule showing the atom numbering scheme. Displacement ellipsoids are drawn at 50% probability level, and hydrogen atoms are shown as small spheres of arbitrary radii.

Dihedral angle between the pyridine ring and the plane of S(1), C(8) and N(2) atoms is 27.8°, indicating that these are not co-planar. The complete details of the geometrical parameters of the ETH molecule are presented in Table S1.†

The crystal structure is stabilized by strong and weak hydrogen bonding interactions. Fig. 3 displays the hydrogen bonding interactions of ETH in the crystal. Each ETH molecule forms three hydrogen bonding interactions [C–H···S$^{(I)}$, and N–H···S$^{(II)}$ and N–H···N$^{(III)}$] with the symmetrically sitting neighbouring ETH molecules in the crystal in which the N–H···N$^{(III)}$ interaction forms an infinite chain along the a-axis, while N–H···S$^{(II)}$ forms an elongated chain approximately 123° from the N–H···N$^{(III)}$ interaction (Fig. 3). The hydrogen bonding parameters of ETH molecule are presented in Table 2

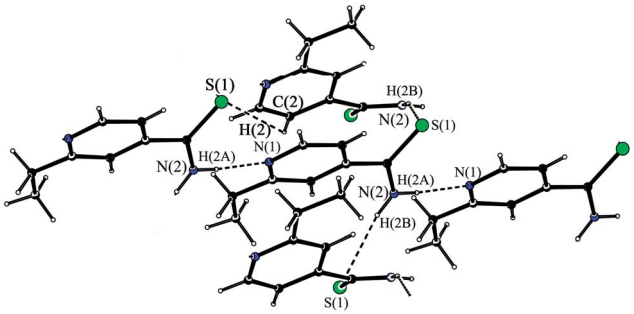

Fig. 3 Hydrogen bonding interactions.

Table 1 Experimental Details

Chemical formula	$C_8N_2H_{10}S$
M_r	166.2
Cell setting, space group	Monoclinic, *Ia*
Temperature (K)	100(2)
a, *b*, *c* (Å)	7.1626(2), 14.9639(3), 7.9231(2)
V (Å^3)	801.01(3)
Z	4
D_x (g cm^{-3})	1.378
Radiation type	Mo Kα
λ (Å)	0.71073
μ (mm^{-1})	0.336
Crystal form, color	Block, yellow
Crystal size (mm)	0.21 × 0.43 × 0.82
Diffractometer	CrysAlisPro, Agilent Technologies, Version 1.171.36.20
Data collection method	\ω-scans
No. of observed reflections	8992
Criteria for observed reflections	$I > 2\sigma(I)$
F(000)	352
R_{int}	0.0406
θ_{max} (°)	52.15
Range of *h*, *k*, *l*	$-15 \rightarrow h \rightarrow 15$, $0 \rightarrow k \rightarrow 33$, $-17 \rightarrow l \rightarrow 17$
Absorption correction	Gaussian ($t_{min} = 0.7711$, $t_{max} = 0.9331$)
Spherical atom model refinement	
$R(F^2)$, $wR(F^2)$	0.025, 0.065
Absolute structure parameter	−0.003(16)
Goodness-of-fit	1.044
No. of reflections used in the refinement	8769
Multipole model refinement	
$R(F)$, $wR(F^2)$	0.018, 0.042
Goodness-of-fit	1.185
N_{ref}/N_v	29.73
No. of reflections	8622
No. of parameters	290
$(\Delta/\sigma)_{max}$	0.0001
$\Delta\rho_{max}$, $\Delta\rho_{min}$ (eÅ^{-3})	0.20, −0.38

[symmetry codes are: (I) $-x$, $-y + 1/2$, $z + 1/2$, (II) x, y, $z - 1$, (III) $x - 1/2$, $-y$, z].

Hirshfeld surface analysis[34] was carried out using Crystal Explorer3.0 (ref. 35) to know the percentage contribution of intermolecular hydrogen bonding interactions of ETH. In ethionamide crystal, C···H contacts contribute the highest percentage of about 50.3%, and the contributions of other intermolecular interactions are found to be in decreasing order; S···H (19.9%), N···H (19.3%), C···C (6.7%), C···N (1.6%) and N···N (0.3%). Thus, C···H contacts contribute the largest fraction for the stabilization of the ethionamide crystal structure.

Table 2 Intermolecular interactions (Å, °)

D–H···A	H···A	D···A	∠D–H···A
C(2)–H(2)···S(1)^a	2.966(15)	3.604	130.0(1)
N(2)–H(2A)···N(1)^b	2.064(15)	2.944	175.2(1)
N(2)–H(2B)···S(1)^c	2.637(15)	3.486	161.8(1)

^{a} (I) $-x$, $-y + 1/2$, $z + 1/2$. ^{b} (II) x, y, $z - 1$. ^{c} (III) $x - 1/2$, $-y$, z.

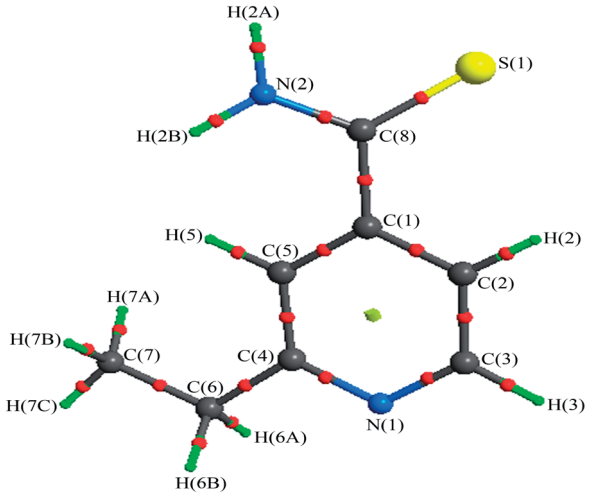

Fig. 4 Molecular graph of ethionamide molecule displays the (3,−1) and (3,+1) critical points. Big circle represents the atomic positions, small circle and square indicates the bond and ring critical points, respectively.

Charge density distribution and chemical bonding

The quality of the refined model was determined by the residual density map and the rigid-bond test.[27] The featureless residual density map (Fig. S1†) shows a good agreement between the observed and the calculated electron densities. The calculated topological properties of electron density allows the qualitative characterization of the covalent bonds, non-bonding interactions and the electronic structure of the molecule. The critical point (cp) search on all the bonds in the molecule revealed a (3,−1) type of critical point named as bond critical point (bcp) for all bonds, which shows their covalent type character.[36] The molecular graph of ETH molecule (Fig. 4) displays the bond and ring critical points. The topological analysis gives the electron density $\rho_{bcp}(r)$ and the Laplacian of electron density $\nabla^2\rho_{bcp}(r)$ at the bcp of each bond in the molecule, which are used to characterize the bond charge concentration or depletion.[37]

The topological properties of the electron density of ETH molecule are presented in Table 3. The electron density $\rho_{bcp}(r)$ of the C–C bonds of ETH molecule containing pyridine ring ranges from 2.01(2) to 2.19(2) eÅ^{-3}, indicating moderate charge accumulation, and the average value is 2.07 eÅ^{-3}; this value is found to be higher than the other C–C [C(4)–C(6): 1.69(2), C(6)–C(7): 1.64(2) and C(1)–C(8): 1.67(2) eÅ^{-3}] bonds of the molecule. Notably, the electron density $\rho_{bcp}(r)$ of S(1)–C(8) bond [1.49(5) eÅ^{-3}] is found to be less than the other bonds in the molecule, and this value is almost close to the reported values.[38,39] Surprisingly, the electron density of C–N [~2.28 eÅ^{-3}] bonds of the ETH molecule contains the pyridine ring and the C(8)–N(2) [2.29(3) eÅ^{-3}] bond is found to be almost equal. The electron density of the C–H bonds of ETH molecule contained in the pyridine ring [~1.91 eÅ^{-3}] is higher than the methyl [~1.81 eÅ^{-3}] and ethyl [~1.76 eÅ^{-3}] C–H bonds. Charge

Table 3 Topological properties of the electron density of ethionamide[a] [first line indicates the experimental value, second line indicates the values obtained from the periodic calculation using the B3LYP/6-31G** method]

Bonds	$\rho_{bcp}(r)$ eÅ^{-3}	$\nabla^2\rho_{bcp}(r)$ eÅ^{-5}	λ_1 eÅ^{-5}	λ_2 eÅ^{-5}	λ_3 eÅ^{-5}	ε	d_1 Å	d_2 Å	R_{ij} Å	Δd%
C(1)–C(2)	2.13(2)	−22.7(5)	−16.4	−12.9	6.6	0.260	0.729	0.671	1.400	2.07
	2.07	−17.3	−14.9	−12.7	10.3	0.17	0.721	0.679	1.400	1.50
C(1)–C(5)	2.01(2)	−19.8(1)	−14.9	−11.7	6.8	0.270	0.702	0.702	1.404	0.00
	2.06	−17.2	−14.9	−12.7	10.3	0.17	0.716	0.687	1.403	1.03
C(2)–C(3)	2.19(2)	−22.9(1)	−16.4	−13.5	7.0	0.210	0.680	0.715	1.394	1.26
	2.12	−18.7	−16.0	−13.1	10.4	0.22	0.683	0.711	1.394	1.00
C(4)–C(5)	2.07(2)	−21.0(5)	−15.6	−11.9	6.5	0.300	0.708	0.694	1.402	0.50
	2.11	−18.3	−15.8	−12.5	10.0	0.26	0.714	0.687	1.401	1.00
C(4)–C(6)	1.69(2)	−13.3(1)	−11.3	−10.0	7.6	0.180	0.812	0.705	1.517	3.53
	1.72	−11.6	−11.3	−10.8	10.5	0.05	0.797	0.718	1.515	2.61
C(6)–C(7)	1.64(2)	−12.2(1)	−10.4	−10.0	7.9	0.080	0.740	0.788	1.528	1.57
	1.58	−8.6	−9.8	−9.8	11.0	0.01	0.767	0.763	1.529	0.13
C(8)–C(1)	1.67(2)	−13.4(1)	−11.7	−10.0	8.2	0.170	0.710	0.788	1.499	2.60
	1.77	−12.3	−12.3	−11.2	11.2	0.09	0.747	0.752	1.499	0.17
C(3)–N(1)	2.29(3)	−28.4(1)	−17.9	−16.4	6.3	0.090	0.520	0.825	1.685	9.10
	2.30	−20.5	−18.5	−15.9	13.8	0.16	0.583	0.761	1.349	6.60
C(4)–N(1)	2.27(3)	−30.3(1)	−17.9	−15.8	3.3	0.130	0.829	0.520	1.349	11.45
	2.28	−20.3	−17.8	−15.2	12.7	0.18	0.771	0.578	1.349	7.15
C(8)–N(2)	2.29(3)	−31.3(1)	−19.7	−17.4	5.8	0.130	0.480	0.849	1.328	13.89
	2.34	−23.3	−18.2	−15.8	10.7	0.16	0.541	0.787	1.328	9.26
S(1)–C(8)	1.49(5)	−7.7(1)	−7.0	−6.30	5.6	0.100	0.822	0.863	1.685	1.22
	1.50	−8.1	−8.4	−6.5	6.7	0.29	0.822	0.864	1.686	1.25
C(2)–H(2)	1.90(7)	−22.0(3)	−17.6	−15.7	11.3	0.120	0.659	0.424	1.083	10.85
	1.87	−19.1	−17.3	−17.0	15.2	0.02	0.700	0.383	1.083	14.64
C(3)–H(3)	2.03(7)	−25.3(3)	−18.3	−17.4	10.4	0.050	0.645	0.438	1.083	9.56
	1.94	−20.0	−19.6	−17.7	17.3	0.11	0.717	0.366	1.083	16.21
C(5)–H(5)	1.79(7)	−17.8(2)	−16.0	−14.2	12.3	0.130	0.657	0.427	1.084	10.61
	1.91	−23.2	−20.2	−17.6	12.4	0.02	0.69	0.378	1.068	14.61
C(6)–H(6A)	1.80(8)	−20.3(2)	−15.8	−13.7	9.2	0.080	0.645	0.448	1.092	9.02
	1.87	−18.5	−16.7	−16.2	14.4	0.03	0.691	0.401	1.092	13.28
C(6)–H(6B)	1.72(8)	−15.4(3)	−13.6	−13.0	11.1	0.050	0.649	0.444	1.093	9.40
	1.82	−16.9	−16.2	−16.1	15.4	0.01	0.704	0.389	1.093	14.41
C(7)–H(7A)	1.90(9)	−17.8(4)	−15.8	−13.6	11.6	0.160	0.637	0.422	1.059	10.15
	1.91	−19.0	−18.1	−17.5	16.7	0.03	0.689	0.369	1.058	15.12
C(7)–H(7B)	1.83(8)	−19.8(2)	−14.9	−13.2	8.3	0.130	0.607	0.454	1.061	7.21
	1.93	−18.9	−18.2	−17.6	17.0	0.03	0.689	0.370	1.059	15.06
C(7)–H(7C)	1.71(8)	−14.3(2)	−12.4	−11.9	10.0	0.050	0.612	0.449	1.06	7.69
	1.99	−20.1	−18.7	−17.9	16.5	0.05	0.677	0.382	1.059	13.93
N(2)–H(2A)	2.30(9)	−28.4(5)	−28.5	−26.8	26.8	0.060	0.709	0.299	1.009	20.32
	2.28	−34.7	−31.8	−30.2	27.3	0.05	0.757	0.252	1.009	25.02
N(2)–H(2B)	2.35(9)	−27.1(4)	−28.3	−27.1	28.3	0.040	0.705	0.304	1.009	19.87
	2.29	−31.4	−35.0	−28.2	27.3	0.09	0.736	0.273	1.009	22.94

[a] $\rho_{bcp}(r)$ and $\nabla^2\rho_{bcp}(r)$, electron density and the Laplacian of electron density at the bcp; λ_1, λ_2, λ_3: eigen values; ε, bond ellipticity; d_1, d_2, the distance between bcp and each bonded atom; D, total bond path length; Δd%, is the percentage of the displacement of bcp from the midpoint of the bond.

accumulation in the amide N–H bonds (2.33 eÅ^{-3}) is relatively higher than those of all the other bonds in the molecule. The deformation density maps (Fig. 5) of the ETH molecule display the different level of charge accumulation in various types of bonds and the position of lone pair electrons of nitrogen atom in the molecule. The negative value of the Laplacian of electron density $\nabla^2\rho_{bcp}(r)$ at the bcp of all the bonds indicates the presence of a covalent interaction between the atoms in the molecule. The Laplacian of electron density of all the C–C bonds of the ETH molecule in the pyridine ring are found to be highly negative when compared with the other C–C bonds present in the molecule; the average negative Laplacian of electron density of the C–C bonds is ∼−21.8 eÅ^{-5}, which confirms that the charges of these bonds are highly concentrated compared to those of the other C–C bonds [C(4)–C(6): −13.3(1), C(6)–C(7): −12.2(1) and C(1)–C(8): −13.4(1) eÅ^{-5}] of the molecule. A similar trend was also observed in the values predicted by theory (Table 3). The $\nabla^2\rho_{bcp}(r)$ value of C–NH$_2$ bond is −31.3(1) eÅ^{-5}, which is slightly higher than the C–N bonds [∼−29.4 eÅ^{-5}] of ETH molecule in the pyridine ring. The $\nabla^2\rho_{bcp}(r)$ value of the S(1)–C(8) bond[40] is −7.7(1) eÅ^{-5}, which is notably less negative. This indicates that the charges of the S–C bond are less concentrated when compared with the other bonds in the molecule, and they are well matched [−7.6 eÅ^{-5}] to

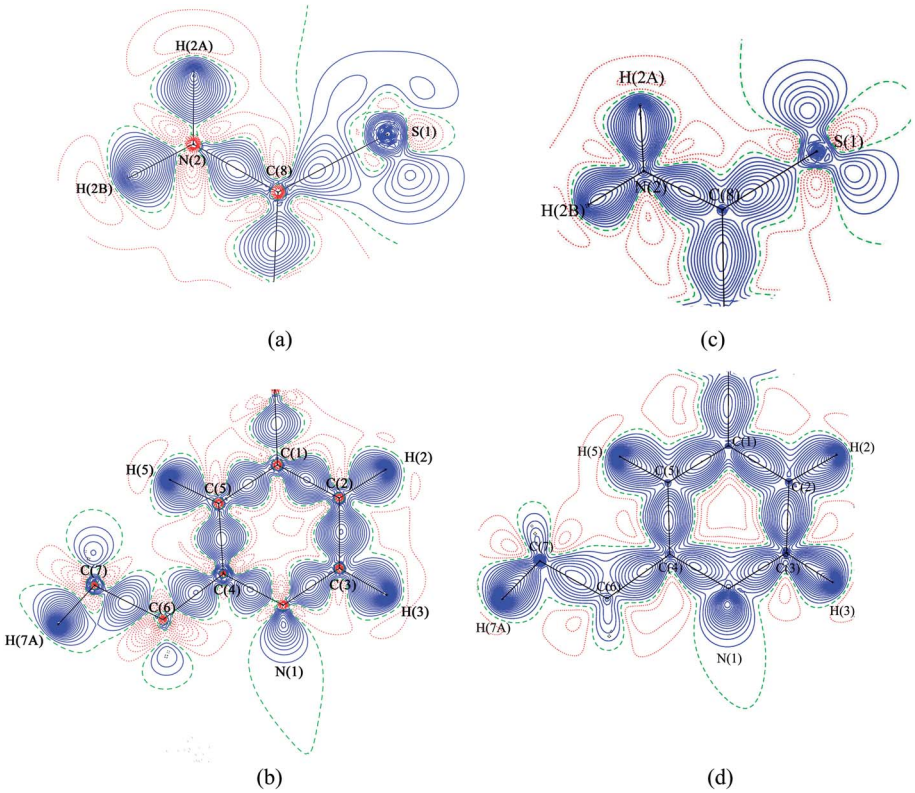

Fig. 5 Experimental (a and b) static and (c and d) theoretical deformation density maps of ethionamide molecule. (a and c) are drawn at C(8), N(2), S(1) plane and (b and d) are drawn at C(1), C(3), C(4) plane. The contours maps are drawn at ±0.05 eÅ^{-3}. Solid blue lines represent positive contours, red dotted lines are negative contours and the green dashed lines are zero contours.

the reported molecule.[40] Furthermore, this value is also slightly less on comparison with the theoretical value (−8.1 eÅ^{-5}) (Table 3).

The Laplacian of the N–H bond is ∼−27.8 eÅ^{-5}, and the large negative value confirms that the charges of the bond are highly concentrated. This value is found to be lower than the theoretically observed values [∼−34.7 and ∼−31.4 eÅ^{-5}]. Overall, there is a small discrepancy found between the theoretical and experimental electron density distribution. This difference can be well understood upon the careful investigation of the eigen values λ_1, λ_2 and λ_3, and it may be due to the different behaviour of Gaussian and Slater-type radial function at the vicinity of bcp and the limited flexibility of basis set and electron correlation effects.[41,42] The values of $\rho_{bcp}(r)$ and $\nabla^2\rho_{bcp}(r)$ of the S–C bond of the ethionamide molecule from both experiment and theory are found to be small, which may be interpreted as a very weak shared interaction between the atoms.[40] The bonding nature of the C and S atoms in terms of charge density distributions of various molecules[38,40,43,44] was analyzed and it was found that the $\rho_{bcp}(r)$, $\nabla^2\rho_{bcp}(r)$ and R_{ij} of the S–C bond of ethionamide molecule are almost similar to 1-formyl-3-thiosemicarbazide; thus, the S–C bond of the ETH molecule shows partial double bond character.[38] This observation indicates the possible resonance character of the S–C bond. Overall, the charge concentration of C–N bonds is predominantly higher than all the other bonds in the molecule, and a similar trend is also observed in theory. Fig. 6 represents

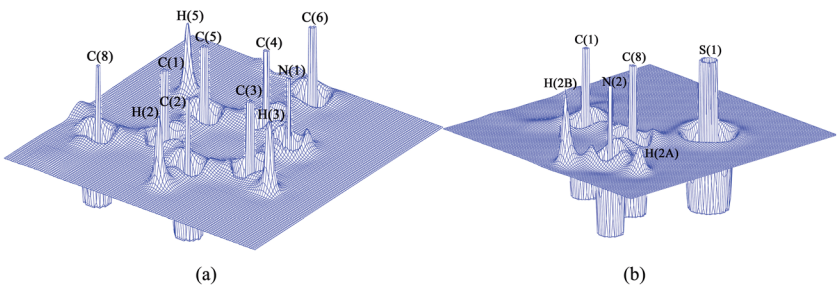

Fig. 6 Experimental relief maps showing the negative Laplacian of electron density of ethionamide molecule drawn in (a) C(1), C(3), C(4) and (b) C(8), N(2), S(1) planes (range −250 to 250 eÅ^{-5}).

Table 4 Atomic charges (*e*) and volumes (Å^3) of ethionamide molecule

	Atomic charges (q_{AIM})		Volume	
Atoms	Experiment	CRYSTAL09	Experiment	CRYSTAL09
C(1)	0.10	0.02	9.9	9.6
C(2)	0.17	−0.03	11.2	11.4
C(3)	0.62	0.29	9.5	10.2
C(4)	0.20	0.33	9.1	8.1
C(5)	0.21	−0.04	9.6	10.1
C(6)	0.31	−0.04	8.4	8.6
C(7)	0.10	−0.15	10.3	10.8
C(8)	0.46	0.25	9.3	9.4
N(1)	−0.98	−0.88	14.6	13.9
N(2)	−0.97	−0.98	16.6	16.2
S(1)	−0.84	−0.29	33.8	32.8
H(2)	−0.02	0.12	6.7	6.4
H(2A)	0.40	0.47	2.6	2.6
H(2B)	0.32	0.43	3.5	3.2
H(3)	−0.04	0.09	6.6	6.3
H(5)	−0.06	0.07	6.2	5.8
H(6A)	0.06	0.06	6.4	7.0
H(6B)	−0.02	0.05	6.5	7.3
H(7A)	−0.12	0.10	7.1	6.6
H(7B)	−0.06	0.08	6.8	6.4
H(7C)	−0.16	0.03	8.4	7.5
			203.1	200.2

the experimental relief map of the ETH molecule. In the relief map, the atom positions are represented by sharp peaks, and the lone pair positions of nitrogen are also clearly visible. The curved surface between the atoms indicates the presence of bonds among the atoms present in the molecule.[45]

The bond ellipticity, ε, of all the bonds in the molecule has been calculated (Table 3), which is a measure of charge accumulation in a plane perpendicular to the bond; it also allows to quantify the π-character and the extent of conjugation in a given molecule.[46] The experimental ellipticity values of all the bonds were found to be higher than the values predicted by DFT calculations. Notably, the ellipticity of the C–C bonds of the ETH molecule in the pyridine ring is ~0.2, which is relatively high when compared with the other bonds in the molecule. This may be attributed to the large anisotropy of electron density and the π-bond nature. The small bond ellipticity values of the S–C and the C–N bonds confirm their cylindrical nature.

Net atomic charges and dipole moment

The experimental AIM charges of atoms and the corresponding atomic volumes of ETH were calculated using TOPXD,[22] and the theoretical charges were calculated using the QTAIM[37] program (Table 4). Among all the atoms, the C(3) and C(8) atoms exhibit high positive charges (0.62*e* and 0.46*e*), while the S(1) and N(1) atoms carry high negative charges, and the corresponding values are −0.84*e* and −0.98*e*, respectively. The methyl hydrogen atoms H(7A) and H(7C) are slightly positive and this trend is also found in the reported paper.[46] The N(2) atom is also negatively charged, and the value is −0.97*e*. This high negative charge tends to have a high positive charge in its attached hydrogen atoms [H(2A): 0.40*e* and H(2B): 0.32*e*]. The atomic volume of carbon atoms ranges from 8.4 to 11.2 Å^3. The sulphur atom is larger in size and its volume is 33.8 Å^3. The volume of hydrogen atoms ranges from 2.6 to 8.4 Å^3, and these values almost match with the reported molecule.[46] The total volume of all the atoms in the unit cell is 812.4 Å^3, and this volume is close to the experimental volume (Table 1) of the unit cell (801.01(3) Å^3) with a difference of 11.4 Å^3. Further, the periodic theoretical calculations also predict a relatively similar volume to the total volume of all the atoms present in the unit cell, and the corresponding value is 800.8 Å^3. The experimental volume of H(2A), H(2B), N(1) and S(1) atoms are 2.6, 3.5, 14.6 and 33.8 Å^3, respectively, and their corresponding theoretical volumes are 2.6, 3.2, 13.9 and 32.8 Å^3, respectively.

Gradient vector field

Fig. 7 shows the gradient vector field of the ETH molecule plotted in two different planes C(1), C(3), C(4) and C(8), N(2), S(1) using the Winxpro software.[47,48] The electron density $\rho_{bcp}(r)$

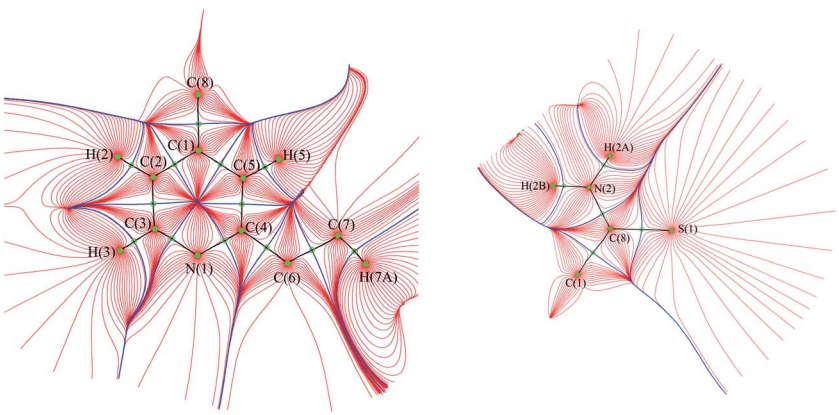

Fig. 7 Gradient trajectory plots of the experimental electron density distribution of the ethionamide molecule drawn in different planes: C(1), C(3), C(4) and C(8), N(2), S(1). The closed blue thick solid lines around an atom are the boundaries of the atomic basin and the green open circles represent the (3,−1) critical points.

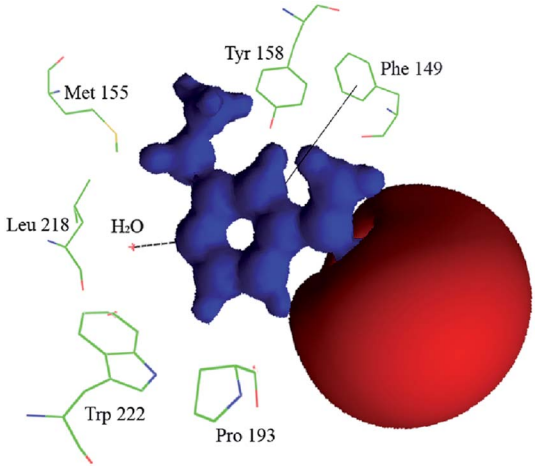

Fig. 8 Isosurface representation of the molecular electrostatic potential map of the ethionamide molecule displays the possible ethionamide–receptor interactions. The positive potential is drawn at +0.5 eÅ^{-1} (blue), and the negative potential is drawn at −0.05 eÅ^{-1} (red).

of a molecule is a scalar quantity and can also be expressed as a gradient vector field. The gradient trajectory originates at the minimum or the saddle point and terminates at the maximum point (atom) *i.e.*, (basin). The basin is surrounded by a zero-flux surface and it is the boundary of the atom, shown in thick blue lines. The carbon atom resembles a prismatic form whereas the sulphur atom resembles a drop. The calculated bond path analysis reveals the polarization of bonds in the molecule. The bcp lies at the middle of the homo atomic bonds and can be viewed in both Fig. 4 and 7. The polarisation in hetero-atomic bonds, such as the C–N bonds can be observed from the position of the bcp, which are moved towards the carbon atom, while in C–H and N–H bonds the bcp positions are shifted towards the electropositive hydrogen atom. Among the non-hydrogen covalent bonds, the C(8)–N(2) bond exhibits maximum polarization, and the degree of polarization is 13.9%. Further, the N–H bonds are found to be highly polar when compared with the C–H bonds. The average degree of polarization of the N–H bond is ∼20.1%.

Electrostatic potential

The electrostatic potential (ESP) of the molecule is one of the derived electrostatic properties of molecules, which is directly related to the reactivity of the molecules.[49] It determines the reactive locations (nucleophilic and electrophilic sites) of the molecule and is also used to predict the alignment of a drug molecule in the active site of its receptor.[50] In the present study, the ESP surface of ETH molecule has been obtained from the experimental multipole modelling; Fig. 8 displays the ESP surface of ETH molecule and interaction (pictorial view) with the neighbouring amino acids present in the active site. Here, the pyridine ring of ETH molecule forms an aromatic π-stacking interaction with the Phe149. The positive surface over the ethyl group of ETH also forms such a π-stacking interaction with the Tyr158. The C(6) atom of the molecule exhibits a high positive charge, which is covalently attached to the NADH to form the ETH–NAD adduct. A large electronegative region is found at the vicinity of the thiocarbonyl atom. The experimental dipole moment of the molecule is 10.6*D*, which is higher than the value predicted by theory [8.2*D*].

Topological properties of electron density of hydrogen bonding interactions

The topological analysis of the electron density of the three hydrogen bonds of ETH molecule (Table 5) was carried out, revealing a (3,−1) type critical point for all the listed hydrogen bonds. The topological properties of hydrogen bonding interactions, local kinetic energy density, potential energy density and local total energy density[51–53] are calculated (Table 5). The calculated energy density and bond dissociation energy (BDE) of the hydrogen bonding interactions at the bcp gives the bond strength.[54] The bcp of C–H⋯S$^{(I)}$ and N–H⋯S$^{(III)}$ hydrogen bonds exhibit a smaller amount of electron density and the values are 0.06(1), 0.07(2) eÅ^{-3}, respectively; the corresponding Laplacian $\nabla^2\rho_{bcp}(r)$ values are found to be positive [0.650(3), 1.15(2) eÅ^{-5}]. The electron density $\rho_{bcp}(r)$ and the $\nabla^2\rho_{bcp}(r)$ values of the N(2)–H(2A)⋯N(1)$^{(II)}$ interaction are 0.18(5) eÅ^{-3}, 1.89(10) eÅ^{-5}, respectively. These values are slightly higher than those of the H⋯S$^{(I)}$ and H⋯S$^{(III)}$ interactions.[55,56] Further, the energetic parameters of C–H⋯S$^{(I)}$ and N–H⋯S$^{(III)}$ are of the order of $|V|/G < 1$ and $H(r) > 0$. From this, it is confirmed that these interactions are closed shell interactions,[57] whereas the energetic parameters for the N–H⋯N$^{(II)}$ are of the order of $|V|/G < 1$ and $H(r) < 0$, which indicates the presence of a partial covalent type of interaction. The BDE of all the hydrogen bonding interactions were calculated (Table 5), in which the N–H⋯N$^{(II)}$ interaction is notably stronger than that of the C–H⋯S$^{(I)}$ and N–H⋯S$^{(III)}$ interactions. Fig. 9 shows the Laplacian of electron density of the C(2)–H(2)⋯S(1)$^{(I)}$, N(2)–H(2A)⋯N(1)$^{(II)}$

Table 5 Topological properties of hydrogen bonds[a]

Interactions	ρ_{bcp}(r) eÅ^{-3}	$\nabla^2\rho_{bcp}$(r) eÅ^{-5}	λ_1 eÅ^{-5}	λ_2 eÅ^{-5}	λ_3 eÅ^{-5}	d_1 Å	d_2 Å	R_{ij} Å	$G(r)$ a.u	$V(r)$ a.u	$H(r)$ a.u	D kcal mol^{-1}
C(2)–H(2)⋯S(1)$^{(I)}$	0.06(1)	0.650(3)	−0.18	−0.13	0.96	1.0416	1.8100	2.8516	0.005	−0.004	0.0006	1.26
N(2)–H(2A)⋯N(1)$^{(II)}$	0.18(5)	1.89(10)	−1.20	−1.16	4.25	1.2928	0.6461	1.9389	0.02	−0.02	−0.0004	6.27
N(2)–H(2B)⋯S(1)$^{(III)}$	0.07(2)	1.15(2)	−0.26	−0.23	1.65	1.7242	0.7949	2.5192	0.009	−0.006	0.003	1.8

[a] $G(r)$, $V(r)$, $H(r)$ represents the kinetic energy density, potential energy density, total energy density respectively; D is the bond dissociation energy. (I) $-x, -y + 1/2, z + 1/2$, (II) $x, y, z - 1$, (III) $x - 1/2, -y, z$.

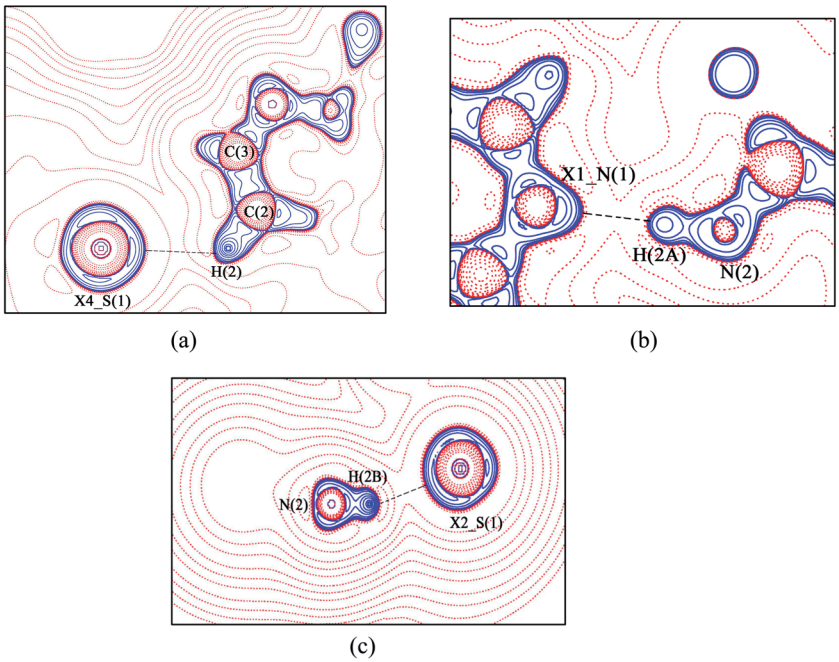

Fig. 9 Laplacian of electron density of (a) C(2)–H(2)···S(1)$^{(I)}$ (b) N(2)–H(2A)···N(1)$^{(II)}$ and N(2)–H(2B)···S(1)$^{(III)}$ hydrogen bonding interactions. Contours are drawn in logarithmic scale, 3.0×2^N eÅ^{-5}, where $N = 2, 4, 8 \times 10^n$, $n = -2, -1, 0, 1, 2$. Solid blue lines and dotted red lines represent positive and negative contours, respectively.

and N(2)–H(2B)···S(1)$^{(III)}$ hydrogen bonding interactions in the crystal [symmetry code: (I) $-x$, $-y + 1/2$, $z + 1/2$, (II) x, y, $z - 1$, (III) $x - 1/2$, $-y$, z].

Conclusions

The topological properties of electron density and electrostatic properties of the ethionamide molecule were determined from the experiment and compared with the periodic theoretical calculations. The charge density distribution of the ETH molecule determined from both the experiment and theory reflects the topological properties of electron density at the bcp of all the bonds in the molecule. Notably, the $\rho_{bcp}(r)$ and $\nabla^2\rho_{bcp}(r)$ of the S–C bond is significantly less than those of all the other bonds in the molecule; this indicates the presence of very weak shared interaction between the atoms and its resonance nature. On the other hand, the electron density at the bcp of the C–N bonds is found to be high, and the charges are also highly concentrated. The S(1) atom has a larger atomic volume than all the other atoms in the molecule. The experimentally determined unit cell volume is similar to the theoretically calculated atomic volume. The N(2)–H(2A)···N(1) interaction is partially covalent type character, while C–H···S and N–H···S exhibit closed shell types of interactions. The charge density analysis of the ethionamide molecule determined from both the experiment and theory gives the topological and the electrostatic properties of the molecule, which allows precise understanding of the nature of intra- and intermolecular interactions.

Abbreviations

inhA	2-*trans* Enoyl acyl carrier protein reductase
ethA	Flavin monooxygenase.
NADH	Nicotinamide adenine dinucleotide hydrogen
INH	Isoniazid
ETH	Ethionamide
MDR	Multi-drug resistance

Acknowledgements

The authors P.K and G.R thanks Prof. T. N. Guru Row for collecting the high resolution X-ray intensity data and also G.R thanks UGC for providing UGC Non-SAP fellowship to carry out this research work.

References

1 M. Flipo, M. Desroses, N. Lecat-Guillet, B. Dirie, X. Carette, F. Leroux, C. Piveteau, F. Demirkaya, Z. Lens, P. Rucktooa, V. Villeret, T. Christophe, H. Kyoung Jeon, C. Locht, P. Brodin, B. Deprez, A. R. Baulard and N. Willand, *J. Med. Chem.*, 2011, **54**, 2994–3010.
2 E. D. Chan and M. D. Iseman, *BMJ*, 2002, **325**, 1282–1286.
3 A. Mahmoudi and M. D. Iseman, *JAMA, J. Am. Med. Assoc.*, 1993, **270**, 65–68.
4 J. Crofton, P. Chaulet, D. Maher, J. Grosset, W. Harris, N. Horne, M. Iseman and B. Watt, *Guidelines for the*

management of multidrug resistant Tuberculosis, World Health Organization, Geneva, Switzerland, 1997, vol. 1.
5 J. S. Blanchard, *Annu. Rev. Biochem.*, 1996, **65**, 215–239.
6 A. E. DeBarber, K. Mdiuli, M. Bosman, L. G. Bekker and C. E. Barry 3rd, *Proc. Natl. Acad. Sci. U. S. A.*, 2000, **97**, 9677–9682.
7 T. A. Vannelli, A. Dykman and P. R. O. Montellano, *J. Biol. Chem.*, 2002, **277**, 12824–12829.
8 J. P. Johnston, P. O. Kane and M. R. Kibby, *J. Pharm. Pharmacol.*, 1967, **19**, 1–9.
9 X. Hanoulle, J. M. Wieruszeski, P. Rousselot-Pailley, I. Landrieu, C. Locht, G. Lippens and A. R. Baulard, *J. Antimicrob. Chemother.*, 2006, **58**, 768–772.
10 P. J. Jenner, G. A. Ellard, P. J. K. Gruer and V. R. Aber, *J. Antimicrob. Chemother.*, 1984, **13**, 267–277.
11 X. Hanoulle, J. M. Wieruszeski, P. Rousselot-Pailley, I. Landrieu, A. R. Baulard and G. Lippens, *Biochem. Biophys. Res. Commun.*, 2005, **331**, 452–458.
12 A. Banergee, E. Dubnau, A. Quemard, V. Balasubramanian, K. S. Um, T. Wilson, D. Collins, G. de Lisle and W. R. Jacobs Jr, *Science*, 1994, **263**, 227–230.
13 A. Quemard, G. Laneelle and C. Lacave, *Antimicrob. Agents Chemother.*, 1992, **36**, 1316–1321.
14 F. Wang, R. Langley, G. Gulten, L. G. Dover, G. S. Besra, W. R. Jacobs Jr and J. C. Sachhettini, *J. Exp. Med.*, 2007, **204**, 73–78.
15 S. Mebs, A. Luth and P. Luger, *Bioorg. Med. Chem.*, 2010, **18**, 5965–5974.
16 S. Grabowsky, T. Pfeuffer, W. Morgenroth, C. Paulmann, T. Schrimeister and P. Luger, *Org. Biomol. Chem.*, 2008, **6**, 2295–2307.
17 M. Mladenovic, M. Arnone, R. F. Fink and B. Engels, *J. Phys. Chem.*, 2009, **B113**, 5072–5082.
18 CrysAlisPro, Agilent Technologies, Version 1.171.36.20 (release 27-06-2012 CrysAlis171. NET).
19 R. H. Blessing, *J. Appl. Crystallogr.*, 1997, **30**, 421–426.
20 G. M. Sheldrick, *SHELXS-97, and SHELXL-97, Programs for Crystal Structure Analysis & refinement (Release 97-2)*, Institut fur Anorganische Chemie der Universitat, D-3400 Gottingen, Germany, 1998.
21 A. L. Spek, *PLATON, A Multipurpose Crystallographic Tool*, Utrecht University, Utrecht, The Netherlands, 1998.
22 T. Koritsanszky, P. Macchi, C. Gatti, L. J. Farrugia, P. R. Mallinson, A. Volkov and T. Richter, *XD-2006. A Computer Program Package for Multipole Refinement and Topological Analysis of Charge Densities and Evaluation of Intermolecular Energies from Experimental or Theoretical Structure Factors, Version 5.33*, 2007.
23 N. K. Hansen and P. Coppens, *Acta Crystallogr., Sect. A: Cryst. Phys., Diffr., Theor. Gen. Crystallogr.*, 1978, **34**, 909–921.
24 D. Chopra, T. N. Guru Row, E. Arunan and R. A. Klein, *J. Mol. Struct.*, 2010, **964**, 126–133.
25 F. H. Allen, O. Kennard, D. G. Watson, L. Brammer, O. Guy and R. Taylor, Tables of Bond length determined by X-Ray and Neutron Diffraction. Part 1 Bond lengths in organic compounds, *J. Chem. Soc., Perkin Trans. 2*, 1987, S1–S83.
26 A. O. Madsen, *J. Appl. Crystallogr.*, 2006, **39**, 757–758.
27 F. L. Hirshfeld, *Acta Crystallogr., Sect. A: Cryst. Phys., Diffr., Theor. Gen. Crystallogr.*, 1976, **A32**, 239–244.
28 R. Dovesi, R. Orlando, B. Civalleri, C. Roetti, V. R. Saunders and C. M. Zicovich-Wilson, *Z. Kristallogr.*, 2005, **220**, 571–573.
29 R. Dovesi, V. R. Saunders, C. Roetti, R. Orlando, B. Civalleri, C. M. Zicovich-Wilson, F. Pascale, B. Civalleri, K. Doll, N. M. Harrison, I. J. Bush, P. D' Arco and M. Llunell, *CRYSTAL09 User's Manual*, University of Torino, Italy, 2009.
30 R. G. Parr and W. Yang, *Density Functional Theory of Atoms and Molecule*, Oxford University Press, London, 1989.
31 P. C. Hariharan and J. A. Pople, *Theor. Chim. Acta*, 1973, **28**, 213–222.
32 L. J. Farrugia, *J. Appl. Crystallogr.*, 1999, **32**, 837–838.
33 M. Alleaume, F. Leroy, M. Gadret and M. Goursolle, *Acta Crystallogr., Sect. B: Struct. Crystallogr. Cryst. Chem.*, 1973, **29**, 1994–2000.
34 J. J. McKinnon, M. A. Spackman and A. S. Mitchell, *Acta Crystallogr., Sect. B: Struct. Sci.*, 2004, **60**, 627–668.
35 S. K. Wolff, D. J. Grimwood, J. J. McKinnon, D. Jayatilaka and M. A. Spackman, *Crystal Explorer 3.0*, University of Western Australia, Perth, 2007.
36 R. F. W. Bader, Y. Tal, S. G. Anderson and T. T. Nguyen-Dang, *Isr. J. Chem.*, 1980, **19**, 8–29.
37 R. F. W. Bader, *Atoms in Molecules: A Quantum Theory*, Clarendon Press, Oxford, NewYork, 1995.
38 P. Munshi and T. N. Guru Row, *Acta Crystallogr., Sect. B: Struct. Sci.*, 2006, **62**, 118–127.
39 V. Tsirelson, A. I. Stash, V. A. Potemkin, A. A. Rykounov, A. D. Shutalev, E. A. Zhurova, V. V. Zhurov, A. A. Pinkerton, G. V. Gurskaya and V. E. Zavodnik, *Acta Crystallogr., Sect. B: Struct. Sci.*, 2002, **62**, 676–688.
40 P. Munshi and T. N. Guru Row, *Acta Crystallogr., Sect. B: Struct. Sci.*, 2006, **62**, 612–626.
41 A. Volkov, Y. Abramov, P. Coppens and C. Gatti, *J. Appl. Crystallogr.*, 2001, **57**, 395–405.
42 H. Birkedel, D. Madsen, R. H. Mathiesen, K. Knudsen, H. P. Weber, P. Pattison and D. Schwarzenbach, *Acta Crystallogr., Sect. A: Found. Crystallogr.*, 2004, **60**, 371–381.
43 P. Munshi and T. N. Guru Row, *Acta Crystallogr., Sect. B: Struct. Sci.*, 2002, **58**, 1011–1017.
44 P. Munshi and T. N. Guru Row, *J. Phys. Chem. A*, 2005, **109**, 659–672.
45 R. V. Williams, V. R. Gadgil, P. Luger, T. Koritsanszky and M. Weber, *J. Org. Chem.*, 1999, **64**, 1180–1190.
46 T. S. Koritsanszky and P. Coppens, *Chem. Rev.*, 2001, **101**, 1583–1628.
47 A. I. Stash and V. G. Tsirelson, *Crystallogr. Rep.*, 2005, **50**, 177–184.
48 A. I. Stash and V. G. Tsirelson, *J. Appl. Crystallogr.*, 2002, **35**, 371–373.
49 D. Stalke, *Chem.–Eur. J.*, 2011, **17**, 9264–9278.
50 P. Politzer and J. S. Murray, *Theor. Chem. Acc.*, 2002, **108**, 134–142.
51 V. G. Tsirelson, *Acta Crystallogr., Sect. B: Struct. Sci.*, 2002, **58**, 632–639.

52 Y. A. Abramov, *Acta Crystallogr., Sect. A: Found. Crystallogr.*, 1997, **53**, 264–272.
53 D. A. Kirzhnits, *Sov. Phys. JETP*, 1957, **5**, 64.
54 E. Espinosa and E. J. Molins, *Chem. Phys.*, 2000, **113**, 5686–5694.
55 U. Koch and P. L. A. Popelier, *J. Phys. Chem.*, 1995, **99**, 9747–9754.
56 P. L. A. Poplier, *Atoms in molecules An Introduction*, Prentice Hall, Harlow, U. K., 2000, pp. 150–153.
57 C. Gatti, *Z. Kristallogr.*, 2005, **220**, 399–457.